Deformation Patterns of Reinforced Foundation Sand at Failure

Radoslaw L. Michalowski, F.ASCE,[1] and Lei Shi[2]

Abstract: While the stability of foundation soils has been written about extensively, the ultimate loads on reinforced soils is a subject studied to a much lesser degree. There is convincing experimental evidence in the literature that metal strips or layers of geosynthetic reinforcement can significantly increase the failure loads on foundation soils. Laboratory tests were performed to investigate the kinematics of the collapse of sand reinforced with a layer of flexible reinforcement. Sequential images of the deformation field under a model footing were digitally recorded. A correlation-based motion detection technique was used to arrive at an incremental displacement field under a strip footing model. Color-coded displacements are presented graphically. The mechanism retains some of the characteristic features of a classical bearing capacity pattern of failure, but the reinforcement modifies that mechanism to some extent. The strips of geotextile used as model reinforcement give rise to the formation of shear bands in a narrow layer adjacent to the geosynthetic. Reinforcement restrains the horizontal displacement of the soil and alters the collapse pattern. The mechanism of deformation identified in the tests will constitute a basis for limit analysis of reinforced foundation soils.

DOI: 10.1061/(ASCE)1090-0241(2003)129:6(439)

CE Database subject headings: Foundations; Soils; Ultimate loads; Deformation; Limit analysis.

Introduction

Failure mechanisms are an important component of stability analysis of earth structures. Mechanisms for some of the structures (for instance, slopes) are well understood, and limit analysis of such structures is reduced to a problem of minimization of the critical height (or the safety factor) with the geometry of the collapse mechanism being variable. When reinforcement is used, the mechanisms become altered, and choosing the right mechanism for stability analysis may not be straightforward. Current experience with reinforced slope failures indicates that the collapse mechanisms are not significantly different from those for natural slopes (Humphrey and Holtz 1986; Porbaha and Goodings 1996), but no such evidence exists for collapse patterns of reinforced foundation soils. Small-scale experimental tests were performed to reveal the deformation pattern of sand reinforced with strips of geotextile. The focus of the experiments was on the progression of the failure mechanism under a footing, and not on the magnitude of the collapse load.

There is extensive evidence available in the literature that metal strips or sheets of geosynthetic material can substantially increase the bearing capacity of footings. Early laboratory experiments of Binquet and Lee (1975) revealed that a failure load on a strip footing founded on sand could be increased by a factor of 2 to 4 when using multiple layers of reinforcement. Reinforcement also reduced the settlement of the footing. Collapse loads on cohesive soils also were found to be increased by the use of reinforcement (Sakti and Das 1987). The advantageous effect of reinforcement was confirmed by field-test experiments by Adams and Collin (1997). While these and many other experiments indicated the benefit of reinforcement in terms of increase in bearing capacity, few studies focused on the mechanics of deformation during the foundation soil failure process. Huang and Tatsuoka (1990) investigated deformation of reinforced sand loaded by a footing. They noticed that the length of reinforcement had a significant effect on the deformation patterns, and they distinguished between a ''deep footing effect'' caused by short reinforcement, and a ''wide slab effect'' associated with reinforcement extending considerably beyond the contour of the footing. Also, Miyazaki and Hirokawa (1992) indicated that the mechanism of deformation under a footing is affected by the presence of reinforcement.

Experimental results reported in this paper focus on the behavior of a granular soil reinforced with one long layer of reinforcement. In particular, the development of localized shear zones is reported, and the interaction of soil and reinforcement is described. It is expected that, once the kinematics of collapse is understood, the limit analysis technique can be applied (Michalowski 1998) to predict the bearing capacity of reinforced soils.

Experimental Tests

Test Container and Loading System

A series of 21 laboratory load tests on strip footings was carried out. Experiments were performed in a test container with transparent (Plexiglas) walls, Fig. 1(a). A large wall thickness was selected (3.81 cm) to avoid substantial deflection during tests. The dimensions of the test container were $61\times61\times30.5$ cm (length $\times$height$\times$thickness). A three-piece aluminum model of a strip

[1]Professor, Dept. of Civil and Environmental Engineering, Univ. of Michigan, 2340 G.G. Brown Building, Ann Arbor, MI 48109-2125. E-mail: rlmich@umich.edu.

[2]Director, National Marketing, World Financial Group, Inc., 11315 Johns Creek Parkway, Duluth, GA 30097.

Note. Discussion open until November 1, 2003. Separate discussions must be submitted for individual papers. To extend the closing date by one month, a written request must be filed with the ASCE Managing Editor. The manuscript for this paper was submitted for review and possible publication on July 10, 2001; approved on May 24, 2002. This paper is part of the ***Journal of Geotechnical and Geoenvironmental Engineering***, Vol. 129, No. 6, June 1, 2003. ©ASCE, ISSN 1090-0241/2003/6-439–449/$18.00.

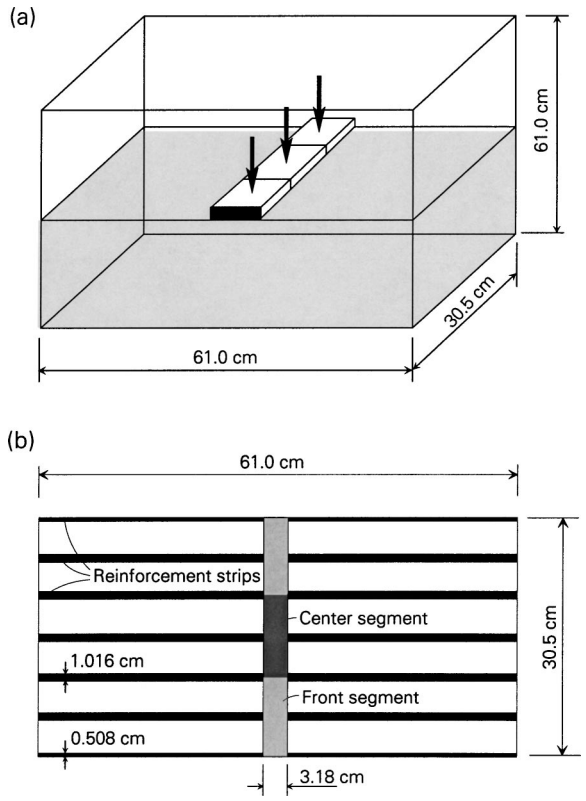

Fig. 1. (a) Test container, and (b) distribution of reinforcement strips

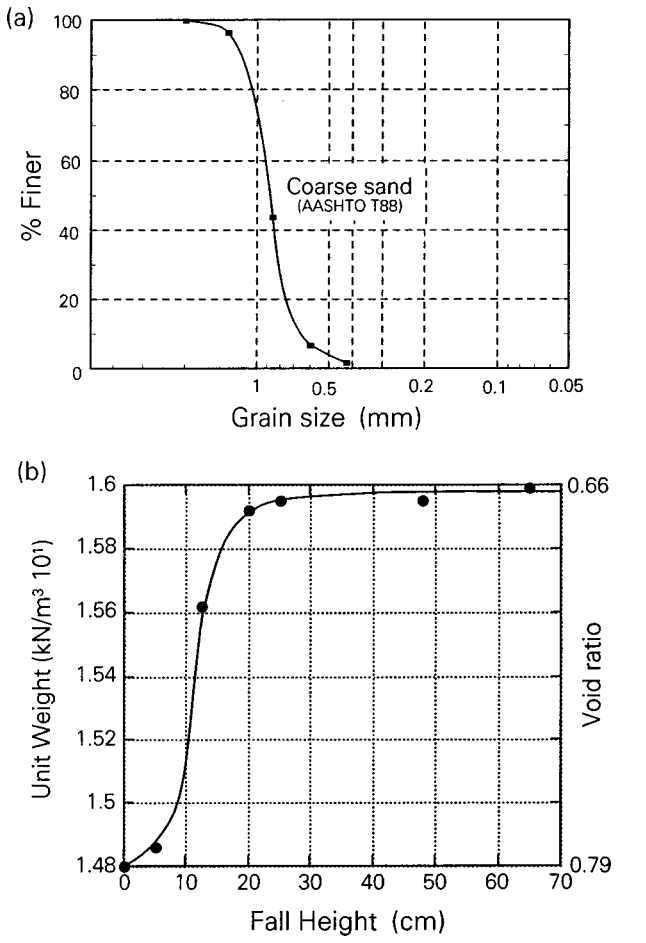

Fig. 2. (a) Grain size distribution, and (b) sand density as function of fall height

footing was used, each piece 10 cm long and 3.18 cm wide. Aluminum blocks were 1.02 cm thick. The three-piece footing model was used to eliminate the effect of wall friction on the indentation force of the center segment of the footing. To provide roughness at the sand-footing interface, a strip of sand paper was glued to the bottom of each segment. Footings of double width (6.35 cm) also were used, but they were found to cause an interference of the failure mechanism with the side walls of the test container, and they led to a ''snap-back'' postpeak behavior, characteristic of a ''soft'' loading system (described in ''Loading of Footings'').

The three segments of the footing were loaded using a lever system with a turnbuckle (kinematic control). The loads on the front and center segments were transferred through proving rings, and the forces were recorded during the footing indentation process.

Material Used

The grain size distribution of sand used in experiments is shown in Fig. 2(a); it is a poorly graded coarse sand (AASHTO T88), with a uniformity coefficient of 1.43 (defined as d_{60}/d_{10}), and maximum and minimum void ratios of 0.89 and 0.56, respectively. This sand was placed in the test container using a sand spreader. The spreader had the shape of a hopper with a width slightly smaller than the container thickness (30.5 cm), and with an opening spanning the entire width of the hopper. The density of the sand bed as a function of the sand fall height from the spreader is shown in Fig. 2(b). Beds with two densities were used in experiments: one prepared with the sand spreader moving just above the surface of the bed, and the second one with the spreader at a height of 15 cm. The first bed corresponds to relative density of $D_r = 0.30$, and the second one $D_r = 0.62$. The internal friction angle tested in direct shear was 34.9° and 44.1°, respectively. These two beds will be referred to as loose and dense, respectively.

The geosynthetic material used in the experiments was a woven polypropylene geotextile with a mass of about 100 g/m^2, thickness of 0.3 mm, tensile strength of 24.5 kN/m, and a negligible resistance to bending (flexible). The interface friction angle tested in a direct shear box was 26.1° and 29.7° for the loose and dense sand, respectively. While the strength of this geotextile would be considered low in a full-scale application, used in a small-scale test this fabric simulates a ''strong'' reinforcement that is expected to slide in the soil rather than rupture. Similarly, the bending stiffness, although negligible in a large-scale application, becomes a factor in a small-scale test. To reduce the influence of the geotextile bending stiffness, strips of the fabric were used rather than a continuous sheet. Prepared sand beds were reinforced with strips of the geotextile in a pattern as shown in Fig. 1(b). The reinforcement area coverage was 20%. The depth of reinforcement varied for different tests.

Loading of Footings

The process of footing indentation was incremental, controlled kinematically, and the resulting forces on two segments of the footing (front and center) were recorded. The displacement (settlement) increments were in the range of about 0.5–2.0 mm, and they could not be kept constant because of the rate-dependent

behavior (creep) of the sand. Since the process was controlled kinematically, time-dependent response of the sand under the footing was causing some relaxation of the force in the loading system. After each increment a pause was taken until the change in forces on the footing in 1 min. became negligible.

Some tests were performed with footings twice the width (6.35 cm) but the results of those tests will not be reported here because of two problems. First, for footings of larger width, the mechanism of collapse for dense sand was found to interfere with the side walls of the test container. Second, larger footings led to a snap-back phenomenon once the process reached the peak load. This occurred because larger footings led to large forces, and this was associated with a substantial increase in elastic energy stored in the loading system. In the postpeak regime, the loading system released the elastic energy as the load declined. Since the rate at which this energy was recovered (for large footing tests) was larger than the ability of the soil to dissipate it, an uncontrollable process (snap-back) occurred.

Motion Detection Technique

Recording of Deformation Pattern

Images of deformed sand under the footing were recorded after each displacement increment with a digital camera with 24-bit color pictures at 1524×1012 pixel resolution. The color pictures were converted to 8-bit grayscale for motion detection computations. The camera was focused on the region of interest at a distance such that, for the poorly graded sand used, the size of grains varied in the range of about 1–4 pixels.

Correlation-based Motion Detection Technique

The purpose of this section is only to indicate the method that was used and not to describe the details of it. Therefore, this description is somewhat sketchy, and the reader is referred to computer science literature for details. The correlation-based method is known also as a block-matching (Pearson 1991), or a region-matching technique (Barron et al. 1993).

An algorithm was adopted here after Anandan (1987). An image of a field is divided into small regions, each described by some intensity distribution function $f_1(x,y)$, and, after a small deformation increment, by $f_2(x,y)$. Cross-correlation function C of the two subregions on two consecutive images is

$$C=\int_{\text{region}}\int f_1(x,y)f_2(x-\delta x,y-\delta y)dx\,dy \tag{1}$$

where x and y = field coordinates, and δx and δy = increments of displacement components. The best estimate of displacement increments is obtained by maximizing function C with δx and δy being variable. This operation was performed for two matching regions (windows) on two sequential images, with functions f having a discrete intensity distribution (constant for each pixel). The candidate match window and the template window were matched using a criterion of minimum squared differences. With the discrete distribution of intensities for the two windows denoted by I and J [which now replace functions $f_1(x,y)$ and $f_2(x,y)$], the matching process of two windows requires minimizing of the following function

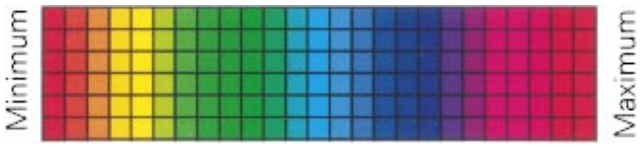

Fig. 3. (Color) Color scale

$$S(x,y,\delta x,\delta y)=\sum_{i=-n}^{n}\sum_{j=-n}^{n}W(i,j)[I(x+i,y+j)-J(x+i-\delta x,y+j-\delta y)]^2 \tag{2}$$

where $W(i,j)$ = weight function; and n = radius of the template window (windows sizes 3, 5, and 7 pixels were used). The computer program used to perform the matching process was a modified computer code (Beauchemin and Barron 1995) that was made available through electronic transmission.

Presentation of Results

Having determined the displacement increments between the sequential images, strain increments were calculated. The displacement increment field was approximated by a nine-node Lagrange biquadratic function

$$\begin{aligned}\delta u_1(x,y)&=a_0+a_1x+a_2y+a_3xy+a_4x^2+a_5y^2+a_6x^2y+a_7xy^2+a_8xy^2\\ \delta u_2(x,y)&=b_0+b_1x+b_2y+b_3xy+b_4x^2+b_5y^2+b_6x^2y+b_7xy^2+b_8xy^2\end{aligned} \tag{3}$$

where δu_1 and δu_2 = horizontal and vertical components of the displacement increment vector. The components of strain increment tensor $\delta\varepsilon_{ij}$ were calculated from

$$\delta\varepsilon_{ij}=\frac{1}{2}\left(\frac{\partial(\delta u_i)}{\partial x_j}+\frac{\partial(\delta u_j)}{\partial x_i}\right),\quad i,j=1,2 \tag{4}$$

and the maximum shear strain and volumetric increments were calculated as

$$\frac{1}{2}\delta\gamma_{\max}=\sqrt{\left(\frac{\delta\varepsilon_{11}-\delta\varepsilon_{22}}{2}\right)^2+\delta\varepsilon_{12}^2} \tag{5}$$

and

$$\delta\varepsilon_v=\delta\varepsilon_{11}+\delta\varepsilon_{22} \tag{6}$$

The main objective of this research was to investigate the mechanism of deformation of the soil under a footing. Thus the vertical and horizontal components of the displacement increment vector field will be presented, as found from the motion detection technique. In addition, the maximum shear strain increment and volumetric strain increments will be reported, as computed from Eqs. (5) and (6).

The displacement and strain increments are color-coded and presented as two-dimensional images. The color scale is shown in Fig. 3. For each quantity to be presented (displacement components, shear strain, volumetric strain), the maximum and minimum values are set at extreme ends of the color scale (Fig. 3). Consequently, the position of a zero displacement component on the color scale depends on the magnitude (absolute value) of the minimum and maximum of that component in the displacement field. Vertical upward and horizontal rightward displacements are

taken as positive. Only if the magnitudes of the maximum (positive) and the minimum (negative) displacement are identical will zero fall in the middle of the scale. Note that the zero shear strain increment will always fall at the extreme left of the scale (red), since as defined in Eq. (5) it is always positive (the minimum is zero). Because the definition of the strain increments in Eq. (4) is consistent with the tension-positive convention, dilatancy here is a positive volumetric strain. The main objective was to investigate the characteristic features of the deformation field in a qualitative manner; therefore the quantitative distribution is not reported directly.

Comments on Tests

While the focus of the experiments was on foundation soil kinematics, the load-displacement curves also are reported. These curves indicate the characteristic features of the loading process (such as monotonic load, or instability), but the magnitude of the loading is not meaningful because of the small scale of the tests.

An interesting study was presented by Tatsuoka et al. (1997) in which the relative size of sand grains (d_{50}) and the footing width (B) were found to have an important effect on the formation of the shear bands (no reinforcement). They found out that propagation of shear bands was a distinct feature of a footing indentation process when B/d_{50} was large, but no shear bands were observed when this ratio dropped to 26. The thickness of localized shear bands depends on the size of the grains (material property), and, increasing the size of the problem promotes a distinct progression of shear band formation, while a small size inhibits this process (see also Michalowski 1990). Ratio B/d_{50} in the laboratory tests performed (36 and 72) was selected such that a propagation of the shear bands was not suppressed, yet the digital motion detection technique could be used with a reasonable computational effort.

Deformation Pattern Under Strip Footing

Four footing indentation experiments were digitally processed to obtain the displacement increment fields. Two of these experiments were without reinforcement (for loose and dense sand), and the remaining two (both dense sand) were with reinforcement at depth $0.4B$ and $0.8B$, respectively (B = footing width). The irreversible deformation process of sand without reinforcement is fairly well understood (Shield 1953). The experimentally investigated deformation field for loose sand is reported here first to illustrate the effectiveness of the method used. Results from the test on dense sand also are presented to make the comparison of foundation soil kinematics for reinforced and unreinforced soil possible.

Some difficulties were encountered in processing information at the free boundary of the deforming sand bed. Because of these problems, the top boundary in the final presentation of the displacement images was truncated with a straight line at the level of footing, and a footing contour was superimposed over that line.

Deformation Process of Loose Sand

Load-displacement curves are shown in Fig. 4 for two model footings. The curve in Fig. 4(a) indicates an average pressure under the center segment of the wide model of the footing (6.35 cm), whereas Fig. 4(b) presents the curves for the front and center segments of the small model (3.18 cm). As expected, the front segment carries a much larger load due to friction on the wall–sand interface. Pressure-displacement curves indicate no peak, as expected for loose sand. The unloading process revealed practically no reversible deformation.

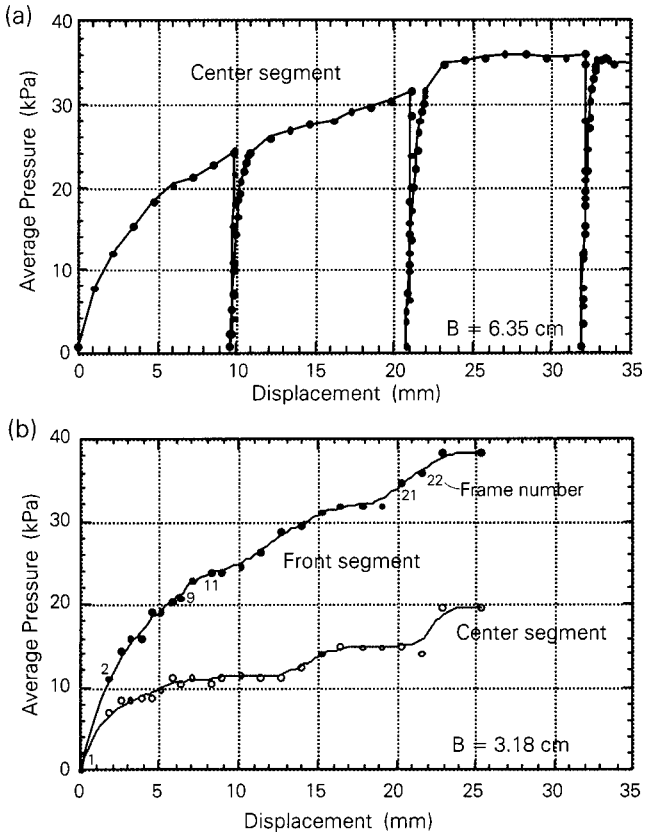

Fig. 4. Load-displacement curves for loose sand; (a) wide footing, and (b) narrow footing

The process of loose sand deformation [for the test in Fig. 4(b)] is illustrated in Figs. 5–7. Instances at which the load readings and digital records were taken are marked in Fig. 4(b) with small circles, and the frame numbers are marked for the increments for which the results are produced in Figs. 5–7. Load readings were taken for both the front and center segments, whereas the experimental setup allowed for digital images to be taken only for the front segment. The length scale on the digitally processed images is related to pixels. The relation of a pixel to the physical model length depends on the digital image resolution and the distance of the camera from the model. The relation of a unit-to-pixel-to-physical length for each set of images is indicated in the upper right-hand part of the figures. The specific relation for Figs. 5–7 is 1 unit of length equals 4 pixels equals 1.32 mm.

Fig. 5 indicates the displacement increment field and the maximum shear strain increment field during the loading interval between the first and second frames. The vertical downward displacement is the largest in a triangular block immediately beneath the footing [Fig. 5(a)], while horizontal displacement of this region is zero [Fig. 5(b)]. The regions to the left and right of the triangular block undergo upward and outward movement. There is a clear initiation of localized shear at the corners of the footing [Fig. 5(c)], and some distributed shear of lesser intensity occurs farther from the footing. This distribution is not quite symmetric, with more distributed shear (yellow) on the left-hand side of the strain field.

Further progress of the deformation pattern is shown in Fig. 6. This displacement increment corresponds to the load interval be-

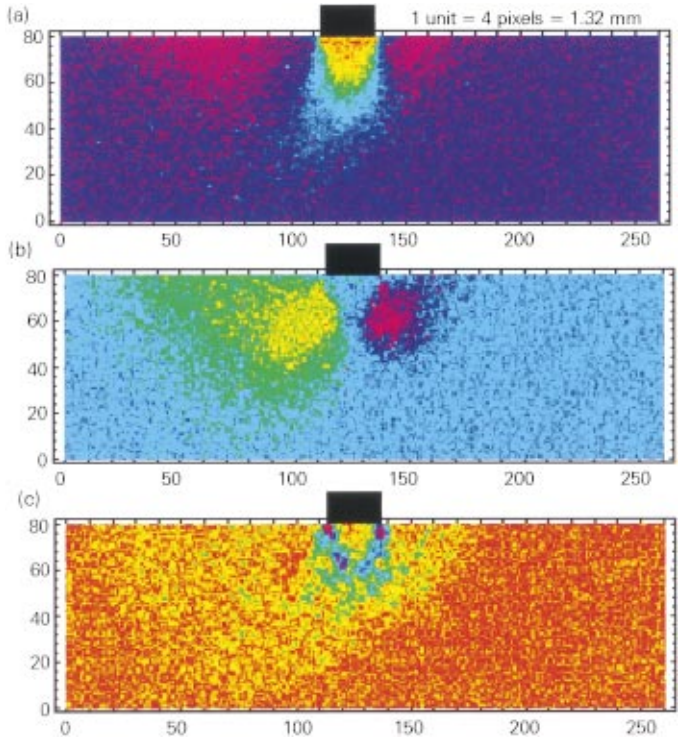

Fig. 5. (Color) Initial deformation of loose sand, interval 1-2: (a) vertical displacement increments; (b) horizontal displacement increments; and (c) maximum shear strain

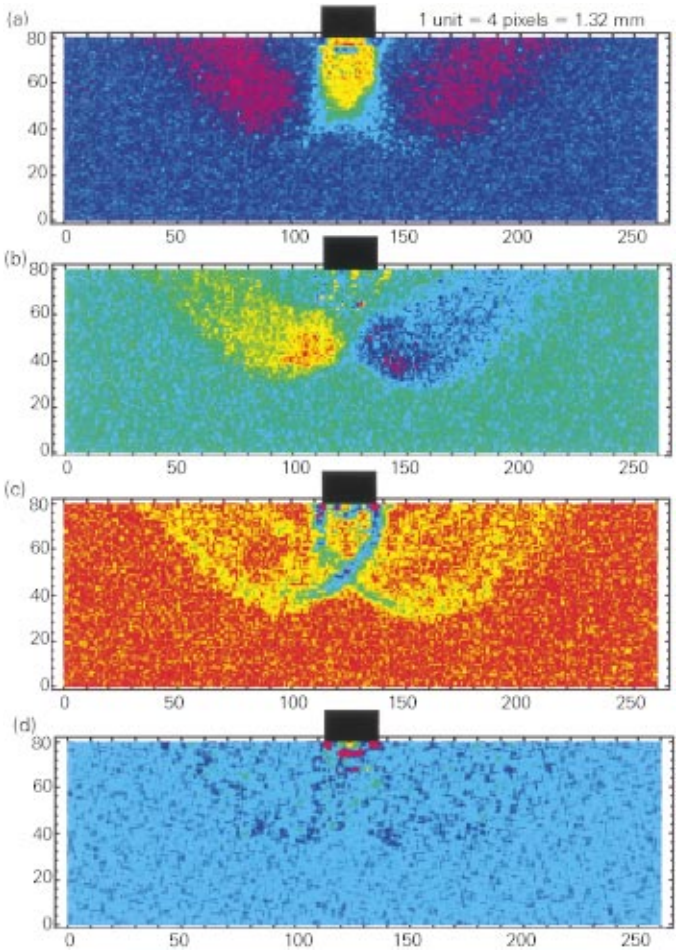

Fig. 7. (Color) Deformation of loose sand, interval 21-22: (a) vertical displacement increments; (b) horizontal displacement increments; (c) maximum shear strain; and (d) volumetric strain increments

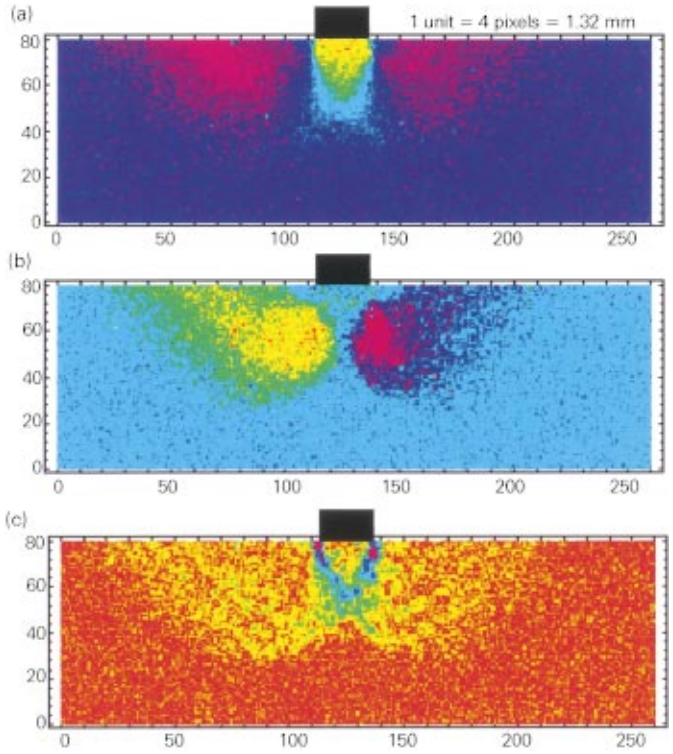

Fig. 6. (Color) Deformation of loose sand, interval 9-11: (a) vertical displacement increments; (b) horizontal displacement increments; and (c) maximum shear strain

tween frames 9 and 11 in Fig. 4(b). The deformation field appears to be symmetric, and its pattern follows the shape of the mechanism associated with the Prandtl (1920) and Reissner (1924) classical slip-line solution to limit pressure over a cohesive-frictional medium (see also Shield 1953; Sokolovskii 1965). The shear bands originating at the corners of the footing intersect at the symmetry axis [Fig. 6(c)], but they do not yet reach the surface of the sand. This pattern persists for a considerable length of the process. The respective increments corresponding to the load interval between frames 21 and 22 are shown in Fig. 7. The pattern of volumetric change is not very distinct, Fig. 7(d). Since the sand was loose to begin with, one would not expect a strong dilation effect associated with shear.

While the deformation pattern looks symmetric, a closer look at the distribution of horizontal increments of displacement indicates that the process oscillates about a symmetric pattern. A ratio of the maximum leftward to the maximum rightward horizontal displacement increments for consecutive load increments is shown in Fig. 8. If the process was perfectly symmetric, then at every load increment this ratio should be exactly equal to 1. Presumably, a larger displacement (and displacement gradient) on one side produces a larger deformation and hardening of the loose sand on that side, which leads to a ''switch'' of the maximum horizontal displacement to the opposite side. This gives rise to an

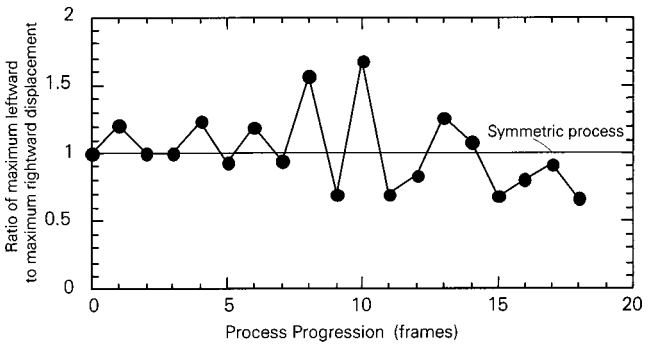

Fig. 8. Ratio of maximum leftward to maximum rightward horizontal displacement increment for loose sand

oscillatory process with a monotonic load increase. Note that the displacement ratio in Fig. 8 does not refer to the displacement of the footing, but to the maximum horizontal displacement in the deforming soil. The displacement ratio in Fig. 8 differs substantially from 1, and the oscillatory process indicated is not likely to be the result of a ''noise'' in the measuring system. One would not expect such a process to occur in a softening medium.

Dense Sand

Load-displacement curves for the indentation process into dense sand are shown in Fig. 9. While the residual load on the center segment of the footing appears to be similar to that for loose sand, the peak load is almost nine times the residual load (this is not indicative of a large prototype footing where the weight of the soil bears more heavily on the limit load).

Increase in displacement and strain during the load interval between frames 4 and 5 is shown in Fig. 10. The extent of the mechanism is now larger than that for loose sand. The region immediately below the footing is subjected to compression, and the gradient of color [Fig. 10(a)] indicates a significant vertical strain. This is predominantly a plastic process; hence the sand dilates [Fig. 10(d)] leading to a substantial horizontal expansion clearly illustrated in Fig. 10(b). There is a substantial distributed shear just below the footing, less intense shear further from the loaded boundary, and shear bands start to form at the corners of

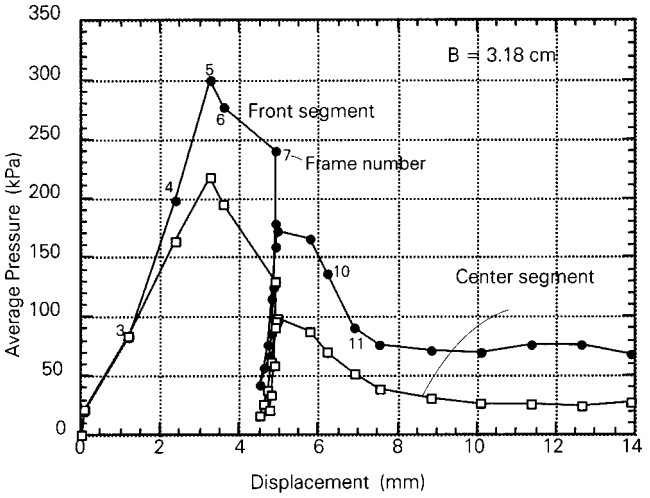

Fig. 9. Load-displacement curves for dense sand

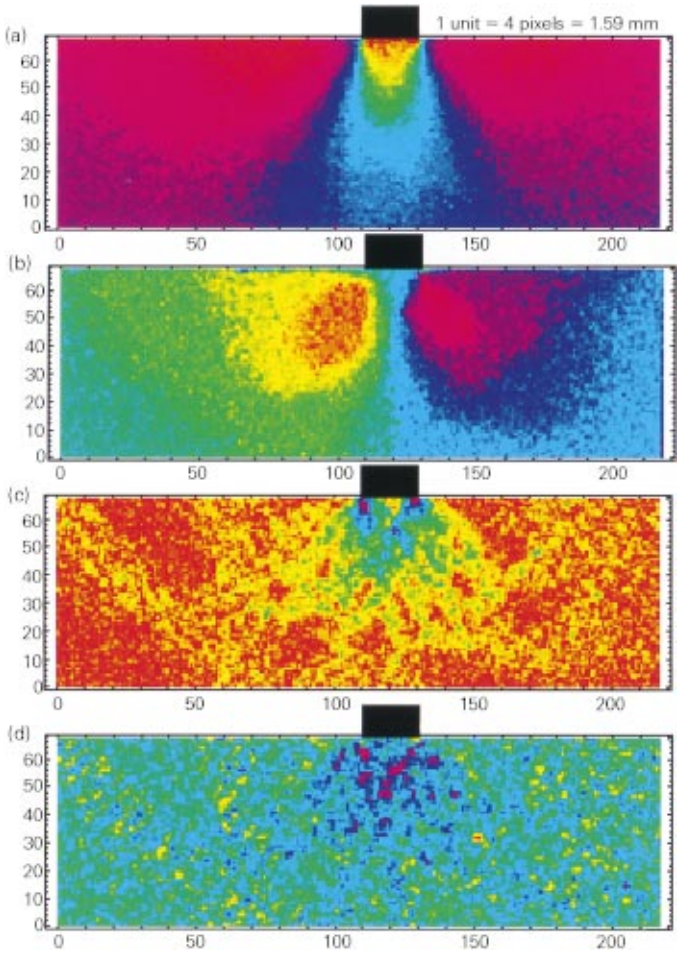

Fig. 10. (Color) Deformation of dense sand, interval 3-5: (a) vertical displacement increments; (b) horizontal displacement increments; (c) maximum shear strain; and (d) volumetric strain increments

the footing [Fig. 10(c)]. The second set of graphs for dense sand includes deformation between frames 6 and 7 of the process (immediately after the peak load). Bands of intense shear have now formed [Fig. 11(c)], and a distinct pattern of dilation (loosening) follows the pattern of shear [Fig. 11(d)]. The process resembles the Prandtl slip-line field, although it is not quite symmetric.

In the subsequent step, the footing was unloaded; the unloading process revealed negligible reversible (elastic) deformation. After reloading, a ''one-sided'' mechanism formed to the right side of the footing, Fig. 12 (frames 10 and 11), with the localized shear band reaching the free surface of the sand bed. This nonsymmetric process is illustrated in Fig. 13. This is not an unexpected result, since the dilatancy in the dense sand is associated with softening of the material, and once the sand softens more on one side of the footing, the process continues in that direction. This is a mode-switching phenomenon, characteristic of deformation processes in strain-softening materials (Michalowski 1990).

Collapse Patterns of Reinforced Dense Sand

Reinforcement Depth 0.4*B*

Load-displacement curves for the front and center segment of the footing are presented in Fig. 14. The increment of deformation between frames 2 and 3 is illustrated in Fig. 15. Vertical displace-

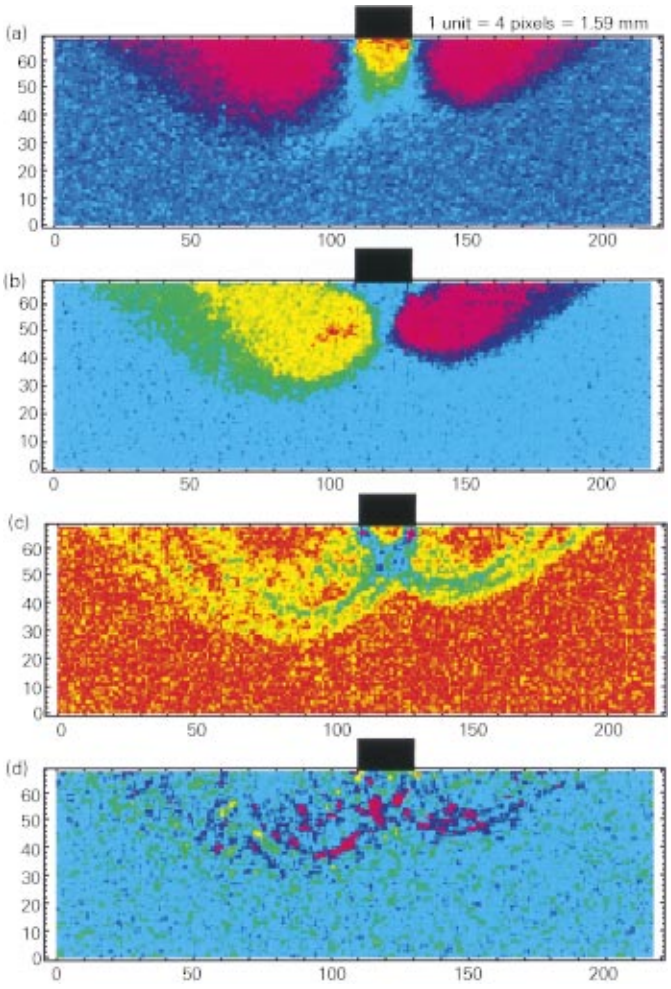

Fig. 11. (Color) Postpeak deformation increment of dense sand, interval 6-7: (a) vertical displacement increments; (b) horizontal displacement increments; (c) maximum shear strain; and (d) volumetric strain increments

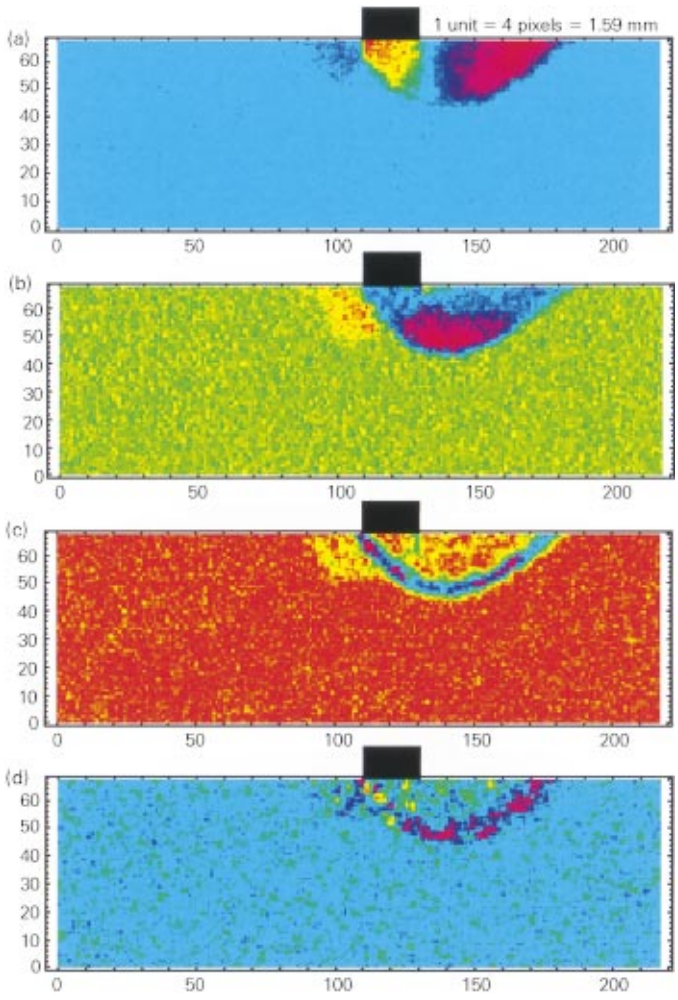

Fig. 12. (Color) Deformation pattern—advanced indentation of dense sand, interval 10-11: (a) vertical displacement increments; (b) horizontal displacement increments; (c) maximum shear strain; and (d) volumetric strain increments

ment appears to be reaching deep into the test container. The maximum downward displacement increment in the field is 1.37 mm whereas the maximum upward displacement is only 0.30 mm, a ratio of 4.6 (consequently, the reddish-purple color in the far field depicts zero vertical displacement; see also Fig. 3). Horizontal displacement of the sand above geotextile appears to be inhibited now by the reinforcement [Fig. 15(b)], while symmetric horizontal movement of sand below the reinforcement is very distinct. The presence of reinforcement gives rise to the formation of symmetric shear bands, which start to propagate in the direction of reinforcement [Fig. 15(c)]. This propagation continues in the prepeak process with a decreasing ratio of maximum downward to upward displacement (1.6 for the interval between frames 3 and 4), and it culminates in a well-defined set of shear bands at the peak load (Fig. 16, frames 5 and 6). The mechanism now does not reach as deep as the pattern in the earlier stage of deformation. A pattern of dilation is visible and it coincides with the shear distribution.

The absence of the horizontal displacement above the reinforcement is an interesting feature of this mechanism. It reduces the work that needs to be expended for relative movement of the soil and reinforcement (reinforcement sliding), but the changes in the mechanism geometry require increased work expenditure

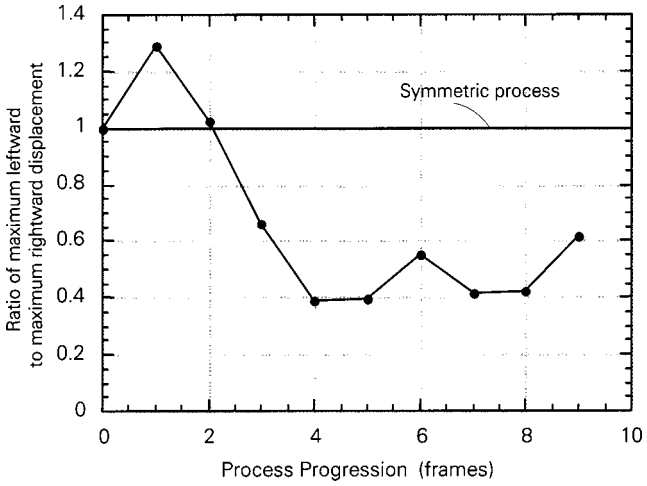

Fig. 13. Ratio of maximum leftward to maximum rightward horizontal displacement increment for dense sand

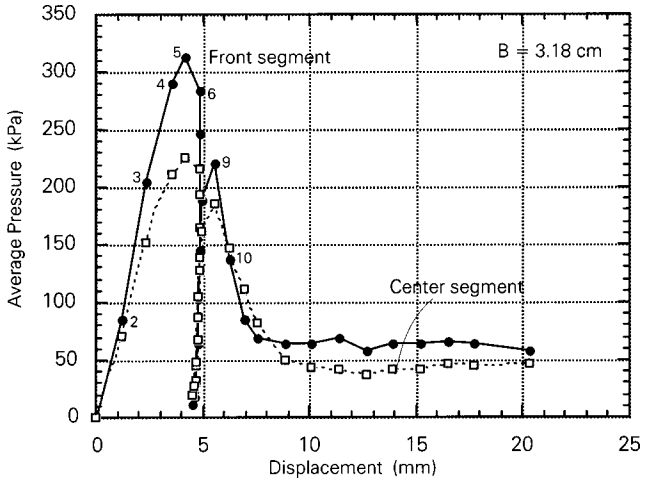

Fig. 14. Load-displacement curves for footing on sand reinforced at depth 0.4*B*

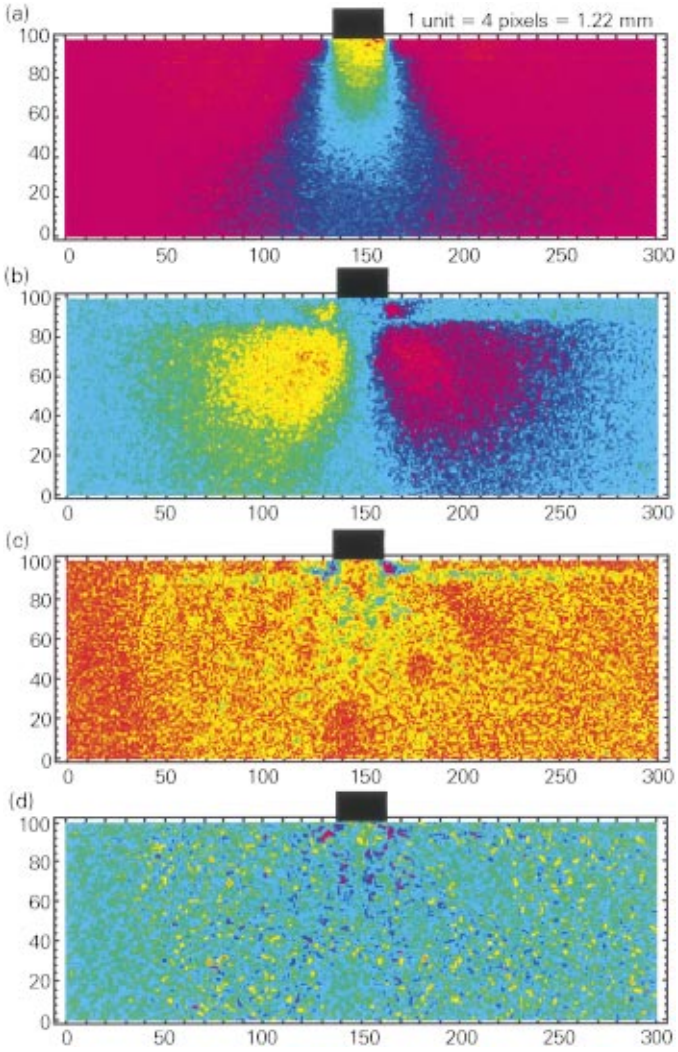

Fig. 15. (Color) Dense sand reinforced at depth 0.4*B*, interval 2-3: (a) vertical displacement; (b) horizontal displacement; (c) maximum shear strain; and (d) volumetric strain

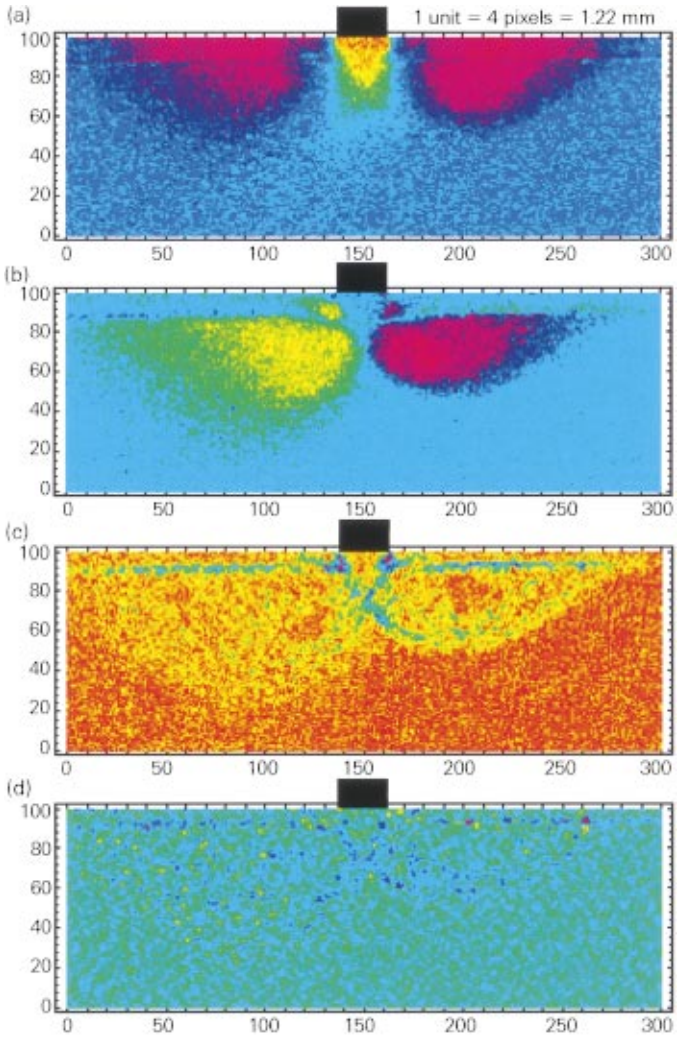

Fig. 16. (Color) Dense sand reinforced at depth 0.4*B*, peak load, interval 5-6: (a) vertical displacement increments; (b) horizontal displacement increments; (c) maximum shear strain; and (d) volumetric strain increments

against the soil weight (when compared to the mechanism in Fig. 11). The second effect dominates for deeper reinforcement and/or larger footings, and the horizontal displacements above reinforcement are not expected to be inhibited in full-size applications.

The footing was subsequently unloaded, and, upon reloading, deformation switched to a nonsymmetric, one-sided mechanism, Fig. 17 (frames 9 and 10). The reinforcement is now being pulled out from the left side of the sand bed, and the dilation along the sheared layer of sand adjacent to the reinforcement causes an upward displacement of sand above the geotextile [Fig. 17(a)], with almost no horizontal displacement [Fig. 17(b)]. At this stage, there is still some vertical and horizontal movement below the reinforcement on the left-hand side, but this will cease later in the process. This distinct pattern, with one shear band extending deep into the right-hand side and the second extending along the interface with reinforcement, persisted through the end of the test.

Reinforcement Depth 0.8*B*

A loading process of sand reinforced at a depth of 0.8*B* is shown in Fig. 18. The initial deformation (frames 3 and 4) reaches deep into the foundation soil [Fig. 19(a)], with reddish-purple being

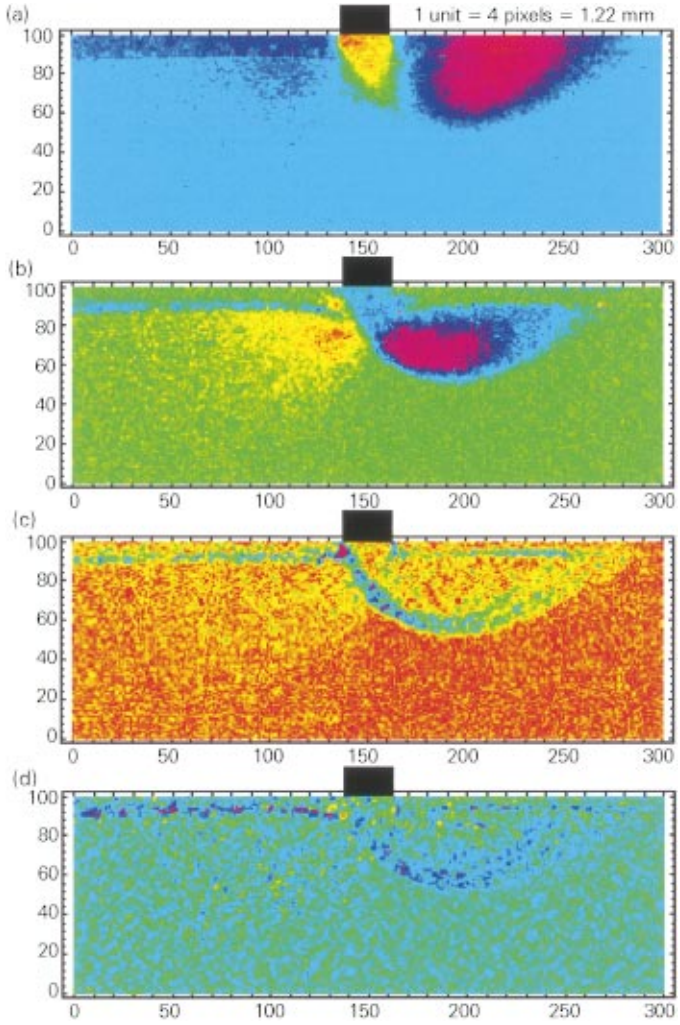

Fig. 17. (Color) Postpeak incremental deformation of sand reinforced at depth 0.4*B*, interval 9-10: (a) vertical and (b) horizontal displacement increments; (c) maximum shear strain; and (d) volumetric strain increments

zero vertical displacement (in this interval, maximum downward displacement was 0.89 mm and maximum upward displacement was 0.22 mm). To some extent, the geotextile now restrains the sand both above and below from moving horizontally [Fig. 19(b)], providing an effective reinforcement outcome. A pair of the shear bands originates at the corners of the footing. These shear bands propagate downward and they divert sideways once they reach the reinforcement [Fig. 19(c)]. This continues during the prepeak process (a similar pattern was recorded during intervals between frames 4–6). A similar pattern with shear bands propagating along the reinforcement can be incurred from a shear strain contour plot shown by Miyazaki and Hirokawa (1992).

Next, the footing was unloaded and reloaded, but the major features of the mechanism did not change (still a prepeak process). Displacement increments at the peak, between frames 11 and 12, are illustrated in Fig. 20. The mechanism became somewhat shallower, but better defined, with a more clear dilatancy distribution. Shortly after (frames 13–15), the deformation pattern switched to a one-sided mechanism, with a distinct region moving to the left [Fig. 21(b)], defined by a shear band separating it from the sand at rest. This pattern persisted through the end of the test, with the geotextile pull out from the right-hand side becoming very distinct.

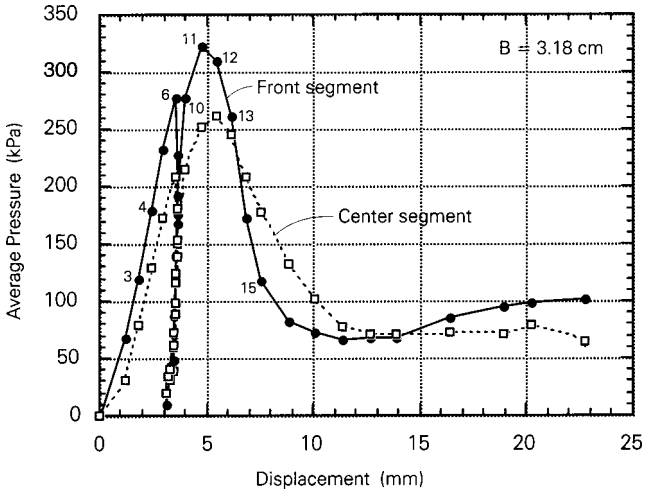

Fig. 18. Load-displacement curves for footing on sand reinforced at depth 0.8*B*

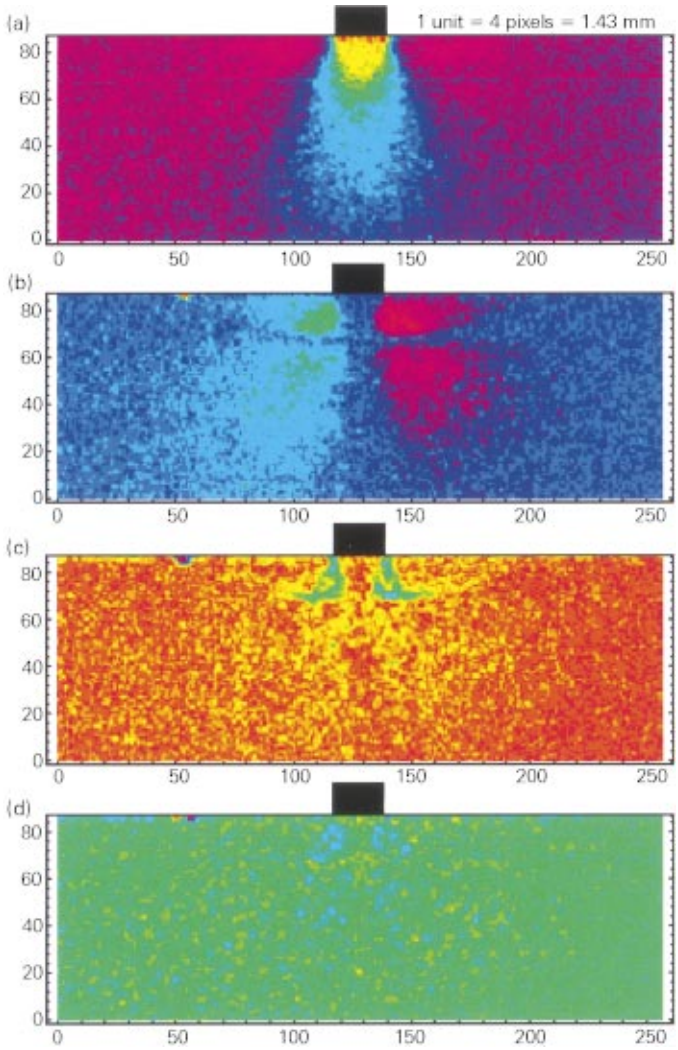

Fig. 19. (Color) Initial deformation pattern of sand reinforced at depth 0.8*B*, interval 3-4: (a) vertical displacement; (b) horizontal displacement; (c) maximum shear strain; and (d) volumetric strain

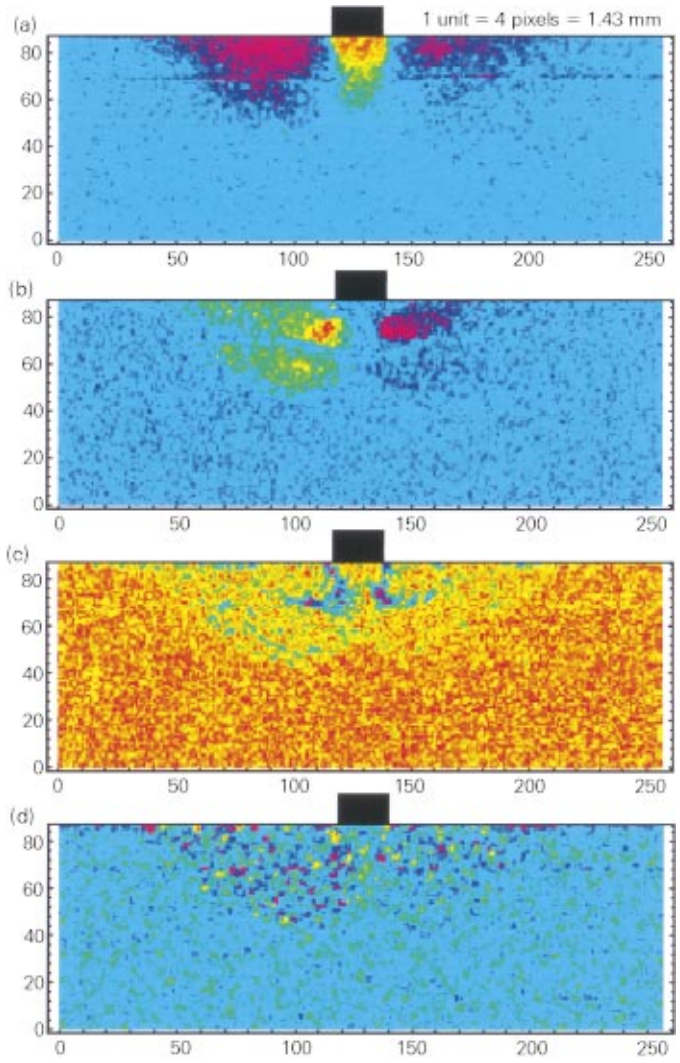

Fig. 20. (Color) Dense sand reinforced at depth 0.8*B*, peak load, interval 11-12: (a) vertical and (b) horizontal displacement increments; (c) maximum shear strain; and (d) volumetric strain increments

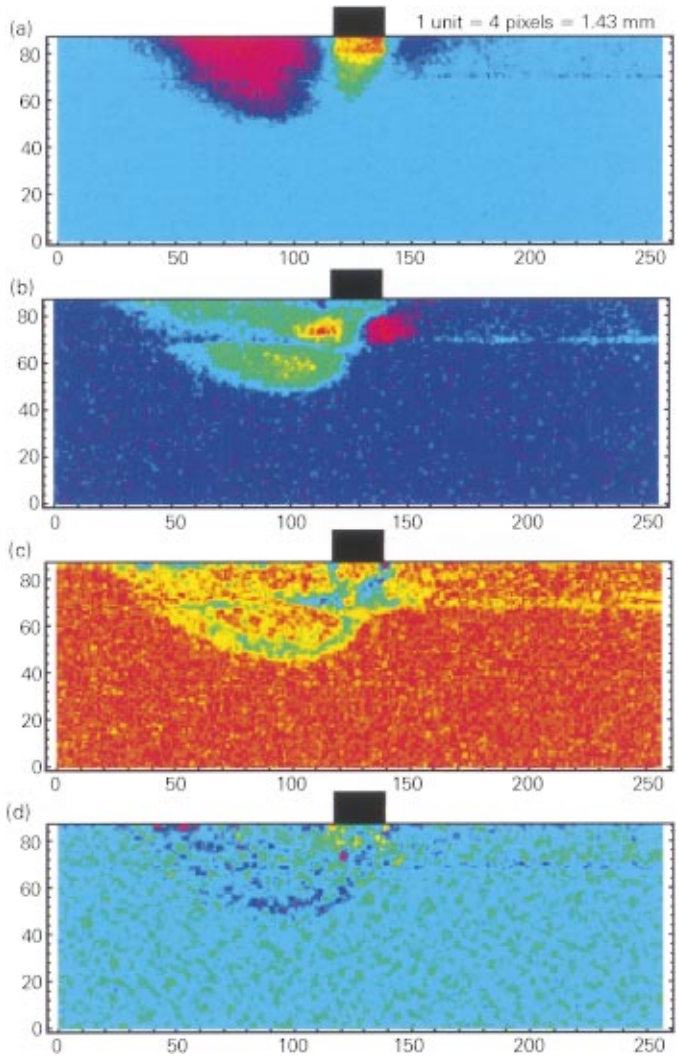

Fig. 21. (Color) Postpeak incremental process of sand reinforced at depth 0.8*B*, interval 13-15: (a) vertical and (b) horizontal displacement increments; (c) maximum shear strain; and (d) volumetric strain increments

Final Remarks

The correlation-based digital technique for motion detection was found to be quite effective in finding displacements from consecutive digital records (snap shots) of the deformation process. The patterns of unreinforced sand deformation under the footing were found to be consistent with those obtained using other techniques (e.g., Tatsuoka et al. 1997), and the digital method was used to investigate deformation patterns of reinforced soil.

Deformation of sand reinforced with one long layer of reinforcement retained many of the features found in sand without reinforcement. Collapse of the sand reinforced with geotextile at a depth of 0.4*B* was associated with the occurrence of two symmetric regions that resemble those found in the classical Prandtl (1920) and Shield (1953) slip-line solutions. However, this mechanism is modified by the presence of reinforcement. While the distribution of vertical displacement is quite similar to that in unreinforced soil, horizontal displacement of sand above the reinforcement is inhibited by the presence of a geotextile. Hence relative sliding of the reinforcement and sand occurs only at the geotextile bottom–side interface, and only in the more advanced phase of deformation is the interface shear fully mobilized. This is manifested by the occurrence of distinct shear bands along the reinforcement. Since the rate of soil-geotextile relative displacement at the bottom–side interface is different from that at the top–side interface, the rate at which the work is dissipated is different at the two interfaces of the reinforcement. This is quite different from the common assumption that the two interfaces contribute equally to stability. This finding is important to constructing admissible mechanisms in limit analysis of reinforced foundation soils. However, this effect may not necessarily be indicative of the failure process for large prototype footings where the weight of the soil bears more heavily on the limit load.

The depth of reinforcement has an important effect on the mechanism formed in sand. At a depth of 0.8*B* the reinforcement causes the propagation of a distinct shear band, inhibiting horizontal displacement of the regions both above and below geotextile. The rates of work dissipation on the two interfaces of the geosynthetic are now equal to one another, and the reinforcement is likely to be more effective.

Reinforcement at depths of both 0.4*B* and 0.8*B* led to a nonsymmetric (“one-sided”) mechanism in the postpeak regime,

with a shear band defining the deformation region on one side and with a clear geosynthetic pull out process from the other side.

The test results presented relate to the case where reinforcement is strong enough so that the collapse of the foundation soil is associated with the slip (pull out) of reinforcement. The case of reinforcement rupture was not considered here. For a given geosynthetic, the distinction between the two cases is very much size-dependent.

The objective of this research was to investigate the failure mechanisms of reinforced foundation soils, so that realistic collapse patterns can be proposed for use in limit state analysis of footings on reinforced soils. It is recognized that small-scale tests are not indicative of limit loads on large-size prototypes. However, the kinematics of failure in large-size processes is likely to have features found in small-size experiments. This was confirmed here in tests of unreinforced foundation soil, where the failure mechanism was found to be consistent with the well-known Prandtl-type pattern. It was found to be true also in tests of other engineering processes involving plastic deformation of granular materials (e.g., silo flow, Michalowski 1987). The mechanisms of failure identified here will be utilized in future work in limit analysis of reinforced foundation soils.

Acknowledgment

The work presented in this paper was supported by the National Science Foundation, Grant No. CMS-0096167. This support is greatly appreciated.

References

Adams, M. T., and Collin, J. G. (1997). ''Large model spread footing load tests on geosynthetics reinforced soil foundations.'' *J. Geotech. Geoenviron. Eng.*, 123(1), 66–72.

Anandan, P. (1987). ''A unified perspective on computational techniques for the measurement of visual motion.'' *Proc., 1st Int. Conf. on Computer Vision*, London, 219–230.

Barron, J. L., Fleet, D. J., Beauchemin, S., and Burkitt, T. A. (1993). ''Performance of optical flow techniques.'' Computer Science Dept., Univ. of Western Ontario, Ont., Canada.

Beauchemin, S., and Barron, J. L. (1995). Computer program made available at the web site of the Computer Science Dept., Univ. of Western Ontario, Ont., Canada.

Binquet, J., and Lee, K. L. (1975). ''Bearing capacity tests on reinforced earth slabs.'' *J. Geotech. Eng.*, 101(12), 1241–1255.

Huang, C. C., and Tatsuoka, F. (1990). ''Bearing capacity of reinforced horizontal sandy ground.'' *Geotext. Geomembr.*, 9(1), 51–82.

Humphrey, D. N., and Holtz, R. D. (1986). ''Reinforced embankments—A review of case histories.'' *Geotext. Geomembr.*, 4, 129–144.

Michalowski, R. L. (1987). ''Flow of granular media through a plane parallel/converging bunker.'' *Chem. Eng. Sci.*, 42(11), 2587–2596.

Michalowski, R. L. (1990). ''Strain localization and periodic fluctuations in granular flow processes from hoppers.'' *Geotechnique*, 40(3), 389–403.

Michalowski, R. L. (1998). ''Limit analysis in stability calculations of reinforced soil structures.'' *Geotext. Geomembr.*, 16, 311–331.

Miyazaki, K., and Hirokawa, F. (1992). ''Fundamental study of reinforcement of sand layer in model test.'' *Proc., Earth Reinforcement Practice*, H. Ochiai, S. Hayashi, and J. Otani, eds., Balkema, Rotterdam, The Netherlands.

Pearson, D. (1991). *Image processing*, McGraw-Hill, London.

Porbaha, A., and Goodings, D. J. (1996). ''Centrifuge modeling of geotextile-reinforced cohesive soil retaining walls.'' *J. Geotech. Eng.*, 122(10), 840–848.

Prandtl, L. (1920). ''Über die Härte plastischer Körper.'' *Nachr. Königl. Ges. Wissensch., Göttingen; Mathematisch-physikalische Klasse*, 74–85.

Reissner, H. (1924). ''Zum Erddruckproblem.'' *Proc., 1st Int. Congress for Applied Mechanics*, C. B. Biezeno and J. M. Burgers, eds., Delft, The Netherlands, 295–311.

Sakti, J. P., and Das, B. M. (1987). ''Model tests for strip foundation on clay reinforced with geotextile layers.'' *Transportation Research Board, 1153*, Transportation Research Board, Washington, D.C., 40–45.

Shield, R. D. (1953). ''Mixed boundary value problems in soil mechanics.'' *Q. Appl. Math.*, 11, 71–75.

Sokolovskii, V. V. (1965). *Statics of granular media*, Pergamon, Oxford.

Tatsuoka, F., Goto, S., Tanaka, T., Tani, K., and Kimura, Y. (1997). ''Particle size effects on bearing capacity of footing on granular material.'' *Proc., Deformation and Progressive Failure in Geomechanics*, IS-Nagoya '97; A. Asaoka, T. Adachi, and F. Oka, eds., Pergamon, 133–138.